Production of Terrestrial Gamma-Ray Flashes During the Early Stages of Lightning Flashes

A. Lindanger[1] , **C. A. Skeie[1]** , **M. Marisaldi[1,2]** , **I. Bjørge-Engeland[1]** , **N. Østgaard[1]** , **A. Mezentsev[1]** , **D. Sarria[1]** , **N. Lehtinen[1]** , **V. Reglero[3]** , **O. Chanrion[4]** , and **T. Neubert[4]**

[1]Department of Physics and Technology, Birkeland Centre for Space Science, University of Bergen, Bergen, Norway, [2]INAF-OAS Bologna, Bologna, Italy, [3]University of Valencia, Paterna, Spain, [4]National Space Institute, Technical University of Denmark, Kgs. Lyngby, Denmark

Abstract Terrestrial Gamma-ray Flashes (TGFs) are short emissions of high energy photons associated with thunderstorms. It has been known since the discovery of TGFs that they are associated with lightning, and several case studies have shown that the TGFs are produced at the initial phase of the lightning flash. However, it has not been tested whether this is true in general. By using the largest TGF sample up to date, combined with ground-based radio lightning detection data, we perform a statistical study to test this. One of the TGF missions is the Atmosphere-Space Interactions Monitor (ASIM) consisting of the innovative combination of X- and gamma-ray detectors, optical photometers and cameras. This allows us to investigate the temporal relation between gamma-rays produced by TGFs and the optical signal produced by lightning discharges. Based on stacking analysis of the TGF sample and ground-based measurements of associated lightning activity, together with the high temporal resolution of the optical signal from the ASIM photometers, it is shown that TGFs are produced in the beginning of the lightning flashes. In addition, for a significant fraction of the TGFs, the lightning activity detected in radio is enhanced in an interval between 150 and 750 ms following the TGFs, and is co-located with the lightning associated with the TGFs. The enhanced lightning activity is not evident in a randomly selected sample of flashes. This indicates that the activity between 150 and 750 ms is a characteristic property of a significant fraction of flashes that start with a TGF.

1. Introduction

Terrestrial gamma-ray flashes (TGFs) are sub-millisecond bursts of energetic photons up to several tens of MeV produced in the atmosphere. The energy spectra of TGFs are compatible with the Relativistic Runaway Electron Avalanche (RREA) process followed by bremsstrahlung emissions (Dwyer, 2003; Dwyer & Smith, 2005; Gurevich et al., 1992; Lindanger et al., 2021; Mailyan et al., 2016). The connection between TGFs and thunderstorm regions has been suggested since the first TGFs were detected by the BATSE instrument onboard the Compton Gamma-ray Observatory (Fishman et al., 1994). TGFs have since been detected from space by RHESSI (Smith et al., 2005), Fermi (Briggs et al., 2013), AGILE (Marisaldi et al., 2010), BeppoSAX (Ursi et al., 2017), the RELEC space experiment on the Vernov satellite (Bogomolov et al., 2017), and ASIM (Østgaard, Neubert, et al., 2019).

Case studies have shown that TGFs can be observed in association with positive Intra-Cloud (IC+) lightning, and several case studies have shown that TGFs are typically produced in the initial phase of lightning flashes during the upward propagation of leaders (Cummer et al., 2015; Lu et al., 2010; Shao et al., 2010; Stanley et al., 2006; Østgaard et al., 2013). Connaughton et al. (2010, 2013) used very low frequency (VLF) radio atmospherics, so-called sferics, produced by lightning and detected by the World Wide Lightning Location Network (WWLLN) together with TGFs detected by Fermi to show that a significant fraction of TGFs is simultaneous with a sferic detection within a few hundred microseconds. This strict association has been confirmed by RHESSI (Mezentsev et al., 2016) and AGILE (Lindanger et al., 2020; Marisaldi et al., 2015). Connaughton et al. (2013) inferred that the radio signal simultaneous with the TGF is produced by the TGF-current itself, and Dwyer and Cummer (2013) modeled this. Østgaard et al. (2021), using a combination of ASIM gamma-ray data, optical data and LF-radio measurements concluded that the TGF-associated radio signal was produced by either the hot-leader lightning channel or the TGF, or a combination of the two. Smith et al. (2016) identified three types of associations between TGFs and sferics; simultaneous association, few milliseconds difference, and those where the radio signals are hundreds of milliseconds after the TGF. The last category will be further investigated in this study.

This likely places the TGF at the beginning of a lightning flash, during the upward propagation of a leader that continues propagating after the TGF. However, this is only based on case studies and has not been shown for a large sample of TGFs. As recent scientific efforts have been focused on the "simultaneity" of TGFs and the temporally closest radio measurement (Connaughton et al., 2010, 2013; Cummer et al., 2011; Lindanger et al., 2020; Mailyan et al., 2020; Marisaldi et al., 2015; Mezentsev et al., 2016), this work will take a step back and focus on TGFs and *all* lightning detections associated to the TGF on 100's ms scale. This will follow up the enhanced lightning activity detected hundreds milliseconds after the TGFs reported by Omar et al. (2014); Smith et al. (2016). Using a large data set of TGF catalogs together with ground-based lightning radio data and optical data from ASIM, we will answer the question: when does the TGF occur in the sequence of discharges constituting a lightning flash and are there any special characteristics with those flashes?

2. Data and Method

This study uses four TGF catalogs from different instruments, lightning data from WWLLN and GLD360, and optical data from the Modular Multispectral Imaging Array (MMIA) instrument onboard ASIM. The TGF catalogs are obtained from the TGF detecting space missions RHESSI, Fermi, AGILE, and ASIM. There are 2824 TGFs (August 2004 to November 2013) from the RHESSI TGF catalog (Smith et al., 2020), 4774 TGFs (August 2008 to July 2016) from the first Fermi-GBM TGF catalog (Roberts et al., 2018), 3473 TGFs (March 2015 to October 2020) from the 3rd AGILE TGF catalog (Lindanger et al., 2020; Maiorana et al., 2020), and 729 ASIM TGFs (June 2018 to September 2020) available from https://asdc.space.dtu.dk. The ASIM instrument is described in detail in Chanrion et al. (2019); Neubert et al. (2019); Østgaard, Balling, et al. (2019). TGFs detected by the same instrument occurring within 5 ms of the previous TGF are removed so that multi-pulse TGFs are counted as a single entry, corresponding to the first TGF. The timing resolution provided by the RHESSI TGF catalog is 1 ms and the absolute timing accuracy is corrected to ~1 ms by the timing correction provided by Mezentsev et al. (2016). The 3rd AGILE TGF catalog is updated including WWLLN-identified TGFs up to October 2020. We also remove TGFs detected by AGILE between July 2015 and December 2017 because AGILE experienced a degradation of the absolute timing accuracy during that period (Lindanger et al., 2020).

Lightning data are obtained from WWLLN (Rodger et al., 2009) and GLD360 provided by Vaisala Inc. (Said & Murphy, 2016). Both lightning networks detect sferics produced by lightning discharges and provides geolocation and timestamps of the sferics. GLD360 also provides peak current values for their detections. WWLLN data from August 2004 and onward are compared to the RHESSI, Fermi, AGILE, and ASIM TGF catalogs. Abarca et al. (2010) and Hutchins et al. (2012) found the location accuracy of WWLLN to be ~5 km for the continental United States, and Østgaard et al. (2013) assumed a global WWLLN location accuracy of 15 km. Comparing WWLLN with Lightning Imaging Sensor (LIS), Bürgesser (2017) estimated a detection efficiency between 1% and 10% for continental regions, and 20% for oceanic regions worldwide. Through the ASIM Science Data Center, GLD360 data are only available for the ASIM mission, therefore it will be used only in association with ASIM data. Using one month of NLDN data over the United States, Said and Murphy (2016) reported the median location accuracy of GLD360 to be ~2 km and the 90th percentile is ~6 km. The detection efficiency was estimated to be ~80% for CG flashes and ~45% for IC flashes.

The time difference between the TGF and the sferic is defined by Equation 1. The time of the sferic is the time of lightning discharge. The propagation time of photons traveling from the lightning location to the satellite is calculated assuming a TGF production altitude of 12 km. Moving three km down or up is only a maximum time difference of 10 μs.

$$\delta t = \text{time}_{\text{sferic}} + \text{time}_{\text{propagation}} - \text{time}_{\text{TGF}} \tag{1}$$

For all the TGFs we keep track of: TGF time and its associated lightning information including the radial distance between the subsatellite point and the location of the sferic source lightning discharge, δt of all sferics, δt of the temporally closest sferic match, and the radial distance between the temporally closest sferic match and the other surrounding sferics. The radial distance is the distance along the surface of the Earth between two coordinates.

Due to instrument sensitivity and efficiency of the various instruments most TGFs are detected within ~500 km from the subsatellite point (Collier et al., 2011; Cummer et al., 2005; Lindanger et al., 2020; Marisaldi et al., 2019; Smith et al., 2016). Therefore, we only consider sferics within 500 km from the subsatellite point to ensure a

Table 1
Overview of the Data Sets and the Sferic Match Criteria Corresponding to Each Space Mission

Instrument	Lightning network	Sferic match criteria	Number of TGFs with sferic match
RHESSI	WWLLN	$|\delta t| < 1$ ms	441
Fermi	WWLLN	$|\delta t| < 0.2$ ms	948
AGILE	WWLLN	$|\delta t| < 0.2$ ms	619
ASIM	WWLLN	0 ms $< \delta t < 30$ ms	230
ASIM	GLD360	0 ms $< \delta t < 30$ ms	477

Note. We require the sferic match to be within 500 km from the subsatellite point.

high signal-to-noise ratio in the stacking analysis. We define a sferic match as the sferic with the smallest $|\delta t|$ value but not larger than the following sferic match criteria. The sferic match criteria depend on the absolute timing accuracy of the instrument we consider. For RHESSI we require δt to be within ± 1 ms, and for Fermi and AGILE we use a sferic match criteria of ± 0.2 ms as their onboard clocks are on microsecond level. The absolute timing accuracy of ASIM varies stochastically between 0 and 30 ms and we chose this as the sferic match criterion. The location of the sferic match is assumed to be the production location of the TGF. An overview of the datasets and their sferic match criteria is shown in Table 1.

This analysis also includes optical data from the MMIA instrument onboard ASIM. MMIA consists of two cameras providing 12 images per second, and three high-speed photometers with a 100 kHz sampling rate. The instrument is described in detail in Chanrion et al. (2019). The two cameras are sensitive in 337.0 and 777.4 nm bands, and the photometers are sensitive in 337.0 nm, 180–240 nm (UV), and 777.4 nm bands. The bandwidths of 337 and 777.4 nm cameras are 5 and 3 nm, respectively. The bandwidths of 337 and 777.4 nm photometers are 4 and 5 nm, respectively. The 777 nm emission is due to atomic oxygen in hot lightning channels and is weakly absorbed in the atmosphere. The UV is strongly absorbed in the atmosphere and is therefore most sensitive to high altitude phenomena such as Elves and other Transient Luminous Events (TLEs). The 337 nm is most sensitive to lightning but will also see some signal from TLEs as it is close to the UV band. The 337 nm is more absorbed in the atmosphere compared to 777 nm. MMIA data acquisition is triggered, and a trigger is generated if the signal is larger than a threshold over a dynamically calculated background. There is also a cross-trigger system that stores MMIA data if the companion instrument, the Modular X- and Gamma-ray Sensor (MXGS), onboard ASIM triggers independently of the MMIA signal. MMIA is only active during nighttime, meaning that we only have optical data for TGFs detected during nighttime. The cameras and the photometers field of view (FOV) is a square 80° diagonal, except the UV photometer that has a circular 80° full cone angle. The relative timing accuracy between MXGS and MMIA was ± 80 µs before March 2019 and ± 5 µs after.

In this study we investigate 71 ASIM detected TGF events with MMIA optical data. These 71 events have been found by Skeie et al., manuscript in preparation, to have optical data associated with the detected TGFs, that is, a clean sample with the TGF produced well inside MMIA FOV and photometer data associated to the TGF. This sample was determined using the photometers, cameras, the high and low energy detector data, as well as lightning sferic activity and TGFs characteristics. For 45 of the TGF events it was also possible to use the GLD360-detected sferics to correct the absolute timing of ASIM down to a few milliseconds, by aligning several photometer pulses with the sferics, similar to what was done in Heumesser et al. (2021); Østgaard et al. (2021); Maiorana et al. (2021).

3. Results

3.1. Stacking Analysis of Lightning Data

To determine whether the TGFs are in the beginning of the lightning flash we did a stacking analysis of sferics. Figure 1 shows a stacking plot of sferics relative to the time of the TGFs, as detected by RHESSI, Fermi, AGILE, and ASIM. The right panels are a close-up version of the left panels. The black histograms shows all sferics without applying the sferic match criteria of Table 1. The first peak at $\delta t \approx 0$ consists mostly of sferics associated with the TGFs. We emphasize that we include *all* sferics within 500 km from the subsatellite point in the stacking analysis, not just the temporally closest sferic. Using a 50 ms bin size means that sferics 25 ms before and after the TGF will be included in the central bin. This implies that the bin will also include some sferics that are not directly associated to the TGF. Note also that the lightning networks sometimes detect the same sferic several times. Therefore, the central bin has more counts than the number of TGFs stacked. Note the enhanced signal from sferics between ~150 and ~750 ms, evident for all instruments. We will call this enhanced signal the "second peak" hereafter. The blue histograms are a sub-selection of events that have a sferic match (Table 1) within 500 km of the subsatellite point, and where only sferics within 20 km radius of the sferic match are included. A schematic of the selection of the two histograms is shown in Figure 2 and the 20 km limit will be
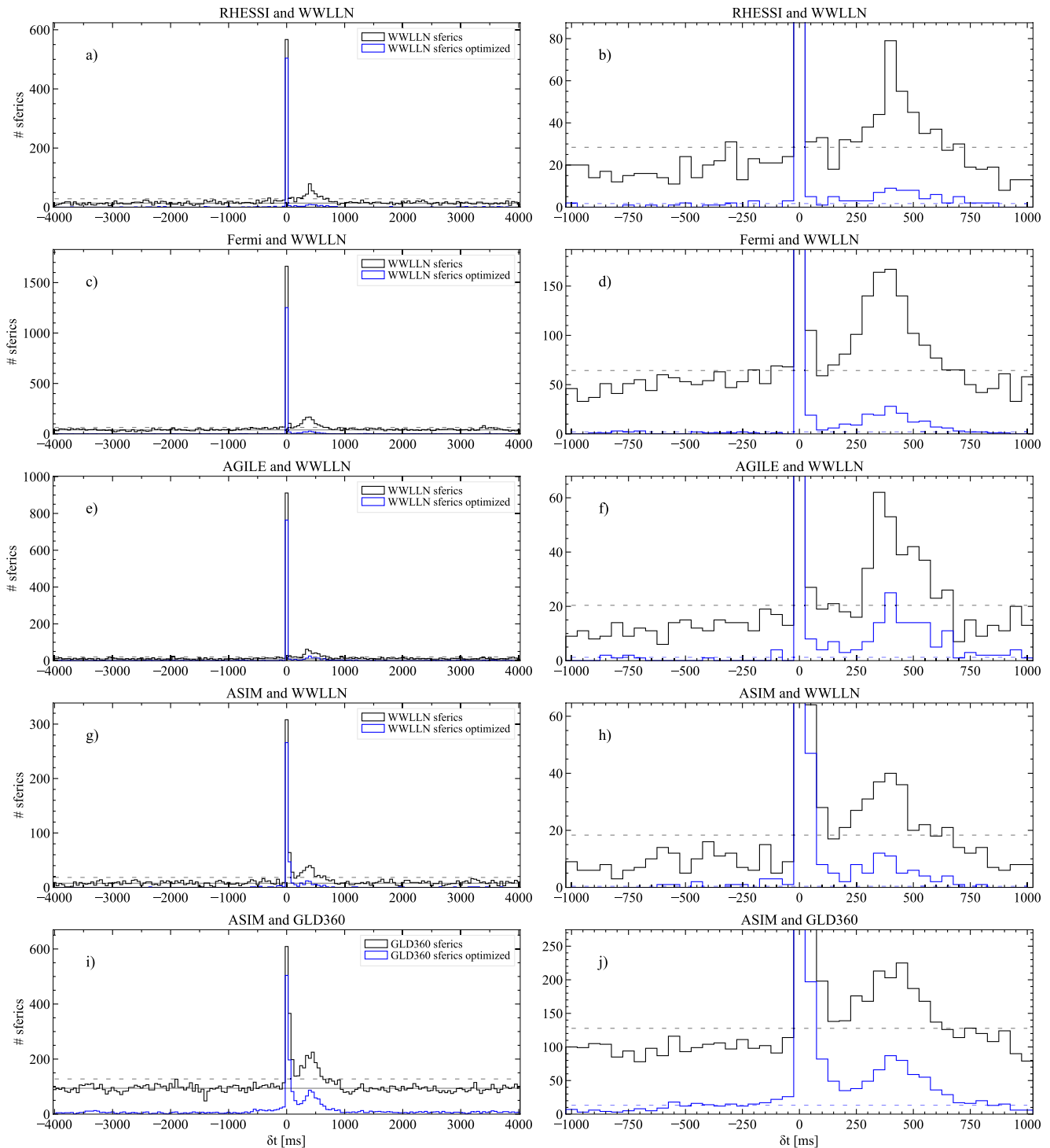
Figure 1. Stacking analysis of sferics as a function of time. $\delta t = 0$ is the TGF time (Equation 1). The right panels are a close-up version of the left panels. The black histograms show *all* sferics within 500 km and the blue histograms show the sferics within 20 km of the TGF-sferic match (Table 1). The selection is illustrated in Figure 2. The solid black line in the left panels is the average background during δt between −4 to −1 s and the black dashed line marks the 3σ level above background assuming Poisson distribution in counts per bin. The dashed blue line in the right panels is 3σ above the background for the blue histograms. Note that the dashed blue line is very close to the *x*-axis for (b, d, f, and h). The bin size is 50 ms.

Figure 2. Figure illustrating the selection of sferics for the black and blue histograms in Figure 1. The black histograms consist of all sferics within $r_1 = 500$ km of the subsatellite point. The blue histograms consist of sferics within $r_2 = 20$ km of the sferic match in the middle of the blue circle in the illustration. The illustration is not to scale.

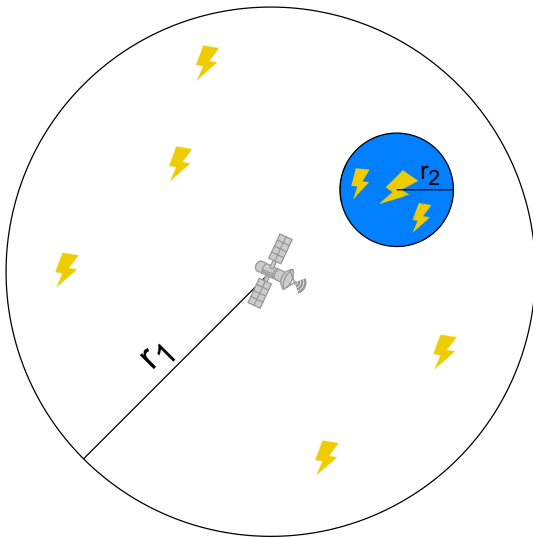justified in the next paragraph. The blue histograms show a higher signal-to-noise ratio for the second peak than the black histogram. The 3σ significance level is shown as a dashed line for the black and the blue histograms. Figure S1 in Supporting Information S1, shows a zoomed view of the same data as in Figures 1c and 1e with a bin size of 50 µs instead of a bin size of 50 ms as in Figure 1.

Figure 3 shows the radial distance between the sferic match and the sferics in the second peak, where the second peak is defined to be δt between 150 and 750 ms. The bin size is chosen so that the area corresponding to each bin is constant, meaning that $A_1 = \pi r_1^2 = A_n = \pi(r_n^2 - r_{(n-1)}^2) = $ constant, where n is the bin index. We see that there is an excess of sferics, within 5–10 km of the location of the sferic match, showing that most activity related to the lightning flash starting with a TGF occur within a radial distance of 20 km. This result is the reason for the 20 km limit to enhance the signal-to-noise ratio in the second peak for the blue histograms in Figure 1.

3.2. Analysis of Optical Data

A sample of 71 ASIM detected TGF events with associated optical data is used to investigate the lightning activity at times close to the TGFs. The TGF production locations are inside the FOV of MMIA. For 13 of the events, several cells were active at the same time of the TGF, which made it impossible to determine at what time they occur in the progression of a flash from measurements by the photometers. One example is shown in Figure S2 in Supporting Information S1. The 13 events are removed from the analysis and we are left with 58 TGF events.

The TGF precedes the large MMIA optical pulse associated with the TGF in 57 cases. Some of the TGFs have a weak optical signal a few milliseconds before the large optical pulse associated with the TGF. This is compatible with lightning leader propagation (Cummer et al., 2015) and has been termed preactivity in earlier studies (Heumesser et al., 2021; Neubert et al., 2020; Østgaard, Neubert, et al., 2019; Østgaard et al., 2021). For the 57 TGFs there are either only one large optical pulse following the TGF (15 events), or there are several optical pulses (42 events) following the pulse associated with the TGF. An example of these is shown in Figure 4. In Figures 4a–4d it is clear that there are no signals detected by MMIA up to ~100 ms before the TGF. The TGF is indicated in (a and b) as a magenta vertical line at time = 0. There is a clear 337 and 777 nm peak associated with the TGF, and following optical pulses are evident in both photometers up to ~400 ms after the TGF. The cropped camera (CHU1 and CHU2) images in Figures 4f and 4g show only one active area that corresponds well with the position of the sferic associated with the TGF in Figure 4e).

In Figure 5, photometer data for 777 nm are shown for 8 (out of 42) TGF events with several pulses following the first pulse associated with the TGF. The TGF time is centered at time = 0, and it is evident that there is no lightning activity before the TGF.

In one of the 58 TGF events, the TGF seems to be in the middle of the flash where we have three optical pulses between 70 and 50 ms before the TGF, not placing the TGF in the beginning of the flash. This TGF event is shown in Figure S3 in Supporting Information S1, and will be discussed later.

4. Discussion

4.1. The TGF Time Relative to the Lightning Flash

Considering first the results of Fermi and AGILE that have the best absolute timing accuracy of ~2 µs, it is clear from Figure 1 that the TGF is produced in the beginning of the flash as there is no signal from sferics before the TGF.
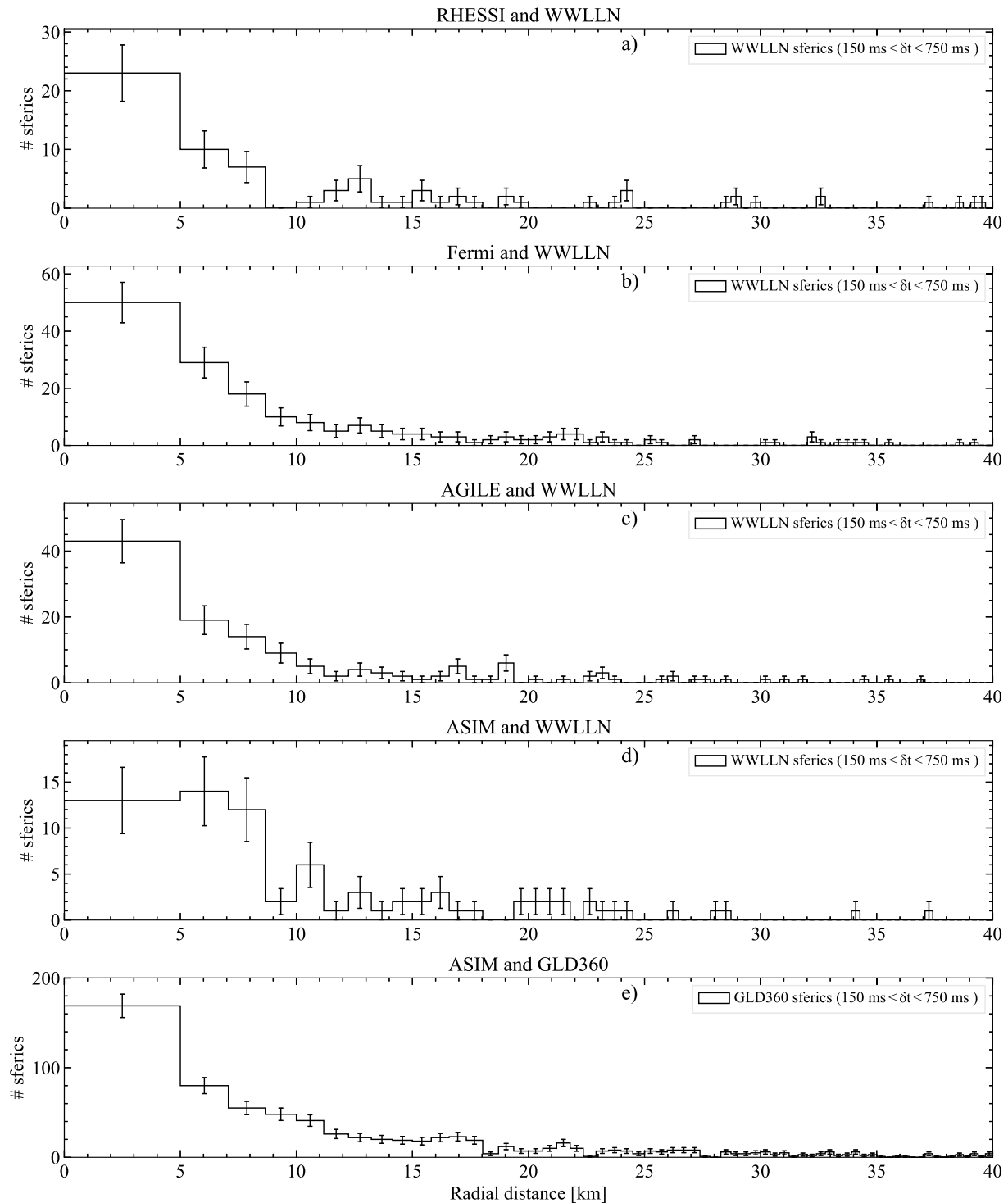
Figure 3. Stack plot showing the radial distance between the sferic matches associated to the TGFs and the sferics in the second peak. The plot shows that most activity related to the lightning flash that starts with a TGF, occur within a radial distance of 20 km. Only TGFs with a sferic match within 500 km of the subsatellite point are stacked. The bin size is chosen so that the area corresponding to each bin is constant. The uncertainty of the data points is ±1 standard deviation assuming Poisson statistics.

The TGFs of ASIM precede the optical pulses for 57 of 58 events left in the analysis. Out of these, 42 are followed by several optical pulses. For these cases it is clear that the TGF is produced in the beginning of the lightning flash. Figure 5 shows examples of 8 of these events. For 15 of the 57 TGFs there are no additional pulses

Figure 4. Overview over MMIA data at the time of a TGF that is in the beginning of a lightning flash. Panels (a and b) show the 337 and 777 nm photometer data with ADC units on the *y*-axis. The vertical black lines indicate t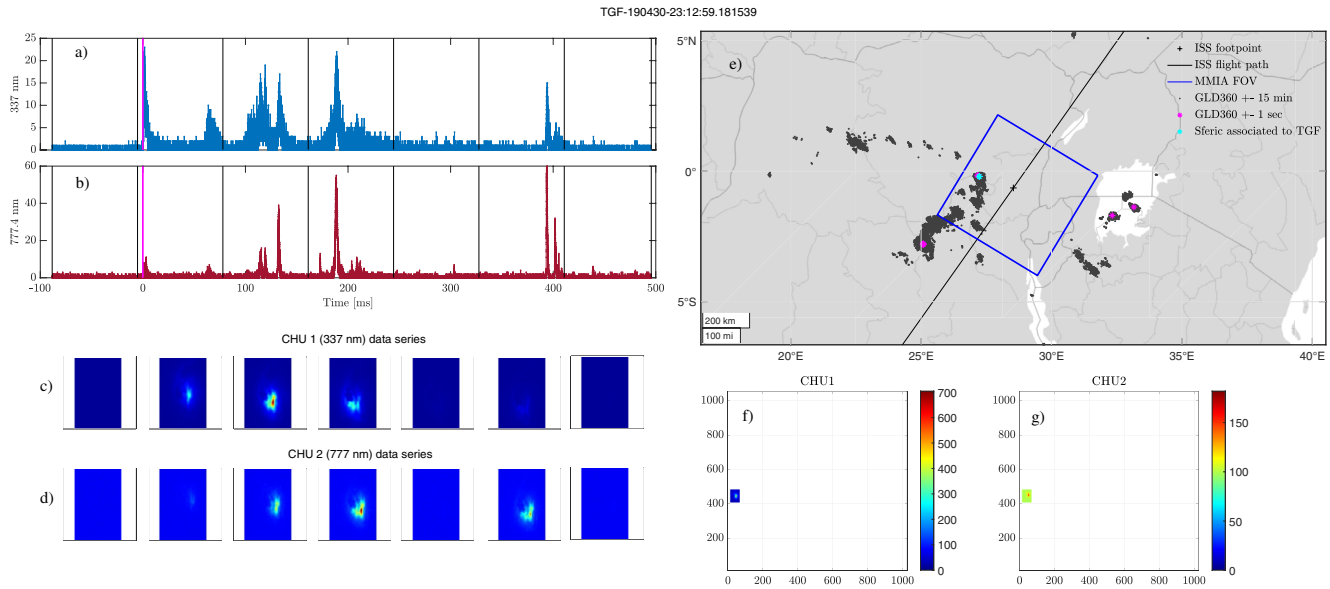he camera frames. The first peak in the 6th frame (~400 ms) in 777 nm peaks at ADC unit 100. The start of the TGF is indicated as a magenta vertical line at time = 0. Panels (c and d) show the corresponding CHU 1 and CHU 2 close-up camera frames. Panel (e) shows a map with MMIA FOV (blue square), ISS position and flight path, and sferics detected by GLD360. The velocity direction of ISS is to the right. Panels (f and g) show the CHU1 and CHU 2 camera frames at the time of the TGF. The full plot is the MMIA FOV and the velocity direction of ISS is in the positive vertical axes.

following the first optical pulse after the TGF. For one event we have optical pulses tens of milliseconds before and after the TGF and its large optical pulse. The time delay between the TGF and the optical pulse is ~1.4 ms. However, we cannot exclude the possibility that the TGF is produced outside MMIA FOV, as there exist active lightning cells outside MMIA FOV as well. This would mean that the detected flash in the photometer data is not correlated with the TGF and it is a chance coincidence. As there is only 1 of the 58 TGFs in the sample with lightning activity before the TGF, it does not change the conclusion that the TGF is produced in the beginning of the lightning flash, especially if we consider that this event may be a timing chance coincidence given the ~1.4 ms delay of the optical pulse relative to the TGF, the active lightning cells outside MMIA FOV, and the rarity of these events in the sample.

Based on the two different, but complementary approaches, where one approach makes use of a large TGF data set with associated sferics, and the other approach makes use of a selected TGF data set with high resolution optical measurements, we conclude that the TGF is produced in the beginning of a lightning flash.

4.2. Increased Lightning Activity After the TGF

It is evident in Figure 1 that we have a second peak of sferics between 150 and 750 ms after the TGF for all TGF catalogs. This is much later than expected for sferics counted twice by lightning detection networks as this happens on less than 100 μs scale, thus it must be a real physical feature of the flashes. After the first peak, at the time of the TGF, the lightning activity decreases almost to background level before it increases again to a local maximum around 400 ms, before it decreases again to the background level. We see that the second peak is significant above 3σ for both black and blue histograms for all space missions. This second peak was first presented by Omar et al. (2014) and discussed in Smith et al. (2016) where it is speculated that the second peak involves cases associated to a subsequent process in the IC flash where horizontal breakdowns occur coupling new charge regions into the already established channel, so-called K-changes. To enhance the signal-to-noise ratio of the second peak, the blue histograms in Figure 1 consist of only TGFs with a sferic match according to Table 1, keeping only sferics within 20 km from the sferic match. Because we require a TGF-sferic match for the blue histogram, the second peak is smaller because we remove TGFs without a sferic match that may have sferics in the second peak. We must remember that a large fraction of TGFs does not have a detectable sferic match (Connaughton et al., 2010, 2013; Lindanger et al., 2020). We can see from Figure 1 that this selection
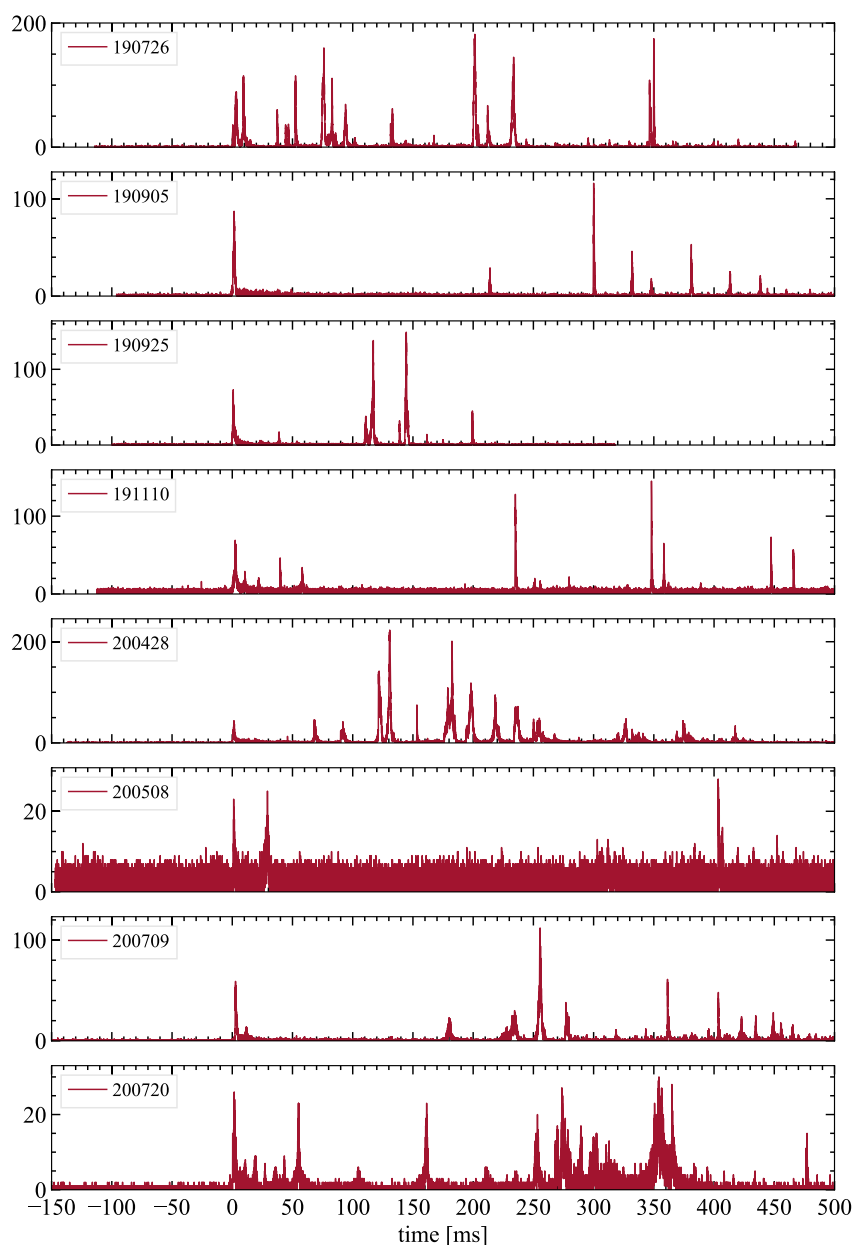
Figure 5. Optical data from the 777 nm photometer for 8 TGFs with lightning activity following the TGF. The TGF time is at time = 0, and the y-axis is in ADC units.

strategy removes almost all the background therefore enhancing the signal-to-noise ratio of the second peak. This is because most of the sferics producing the second peak are not located farther than 20 km from the sferic match. At a resolution of less than 20 km we approach the global location accuracy of WWLLN and GLD360, and from Figure 3 we can see that the 20 km radial distance from the TGF-sferic match is a conservative upper limit. Thus, we conclude that the second peak is co-located with the first peak within the localization uncertainties of the lightning detection networks meaning that the lightning discharges producing the second peak are co-located with the production location of the TGF. Note that Figure 5 shows a wide variability of the lightning activity, as observed in the optical bands, following the TGF, and that a second peak can only be seen on a larger sample of TGFs as shown in Figure 1.

To investigate if all TGFs with a sferic match (blue histograms in Figure 1) also have a sferic contributing to the second peak, we calculate the fraction of TGFs that also has one or more sferics in the second peak, between 150

Table 2
Overview Over the Fraction of TGFs With a Sferic Match That Also Have Sferic Detections in the Second Peak

Instrument-network	# TGFs with a sferic match and activity in 2nd peak	Fraction relative to 1st peak
RHESSI-WWLLN	44	0.10
Fermi-WWLLN	118	0.12
AGILE-WWLLN	83	0.13
ASIM-WWLLN	41	0.18
ASIM-GLD360	243	0.51

Note. The fraction is calculated by dividing the second column by the last column in Table 1.

and 750 ms. The results are shown in Table 2 and reveal that on average 13% of the TGFs with a WWLLN-sferic match also have sferic activity in the second peak. The fraction of TGFs with activity in second peak increases from RHESSI to ASIM. This can be explained by the improvement of the detection efficiency of WWLLN over time as the instruments are sorted from the oldest to newest time span of TGF detections. It is interesting to note that comparing ASIM-WWLLN with ASIM-GLD360, 18% of the TGFs with WWLLN-sferic matches have WWLLN detected sferics in the second peak, while 51% of the TGFs with GLD360-sferic matches have GLD360-detected sferics in the second peak. This can be explained by the difference in detection efficiency and sensitivity for the lightning detection networks. The median absolute peak current value, provided for GLD360 detections, for the first peak is 30 kA, and the median value for the second peak is 12 kA. As the strokes in the second peak in general have smaller peak currents than the first peak, the strokes in the second peak are harder to detect by lightning detection networks. This means that the detection of strokes in the second peak is strongly dependent on the sensitivity of the detection network, that is, in the threshold peak current. This is a further confirmation that when TGFs are compared to lightning data provided by lightning detection networks, the results are heavily affected by the networks' detection efficiency and sensitivity.

Mailyan et al. (2020) report a median peak current of 82 kA for sferics simultaneous with the TGFs within ±200 µs, and a median peak current of 26 kA for sferics associated with the TGFs from 200 µs to 3.5 ms, before and after the TGF. The median value of 30 kA in the first peak in Figure 1i consists of sferics ±25 ms relative to the TGF, therefore including non-simultaneous sferics, biasing the median value toward lower values. Due to the timing uncertainty of ASIM, this study cannot reproduce the median peak current values from Mailyan et al. (2020).

To check if the second peak is unique for TGF production, or just a common feature of lightning flashes, we did a blind search in the GLD360 data for the first stroke in a lightning flash. The blind search data were downloaded independent of ASIM TGF triggers. We defined the first stroke in a flash as the first sferic that had no other detected sferics up to 2 s before within a radial distance of 800 km. This is done for randomly selected GLD360 data between $\pm23°$ latitude identifying 167 300 flashes with a total of 515 399 detected strokes/sferics. We did the same stacking analysis as we did for TGFs, stacking all sferics superposed at the time of the first lightning stroke. The results are shown in Figure 6 where we plot the sferics within 20 km following the first stroke, not including the first stroke itself, with the same time bin of 50 ms as used for Figure 1. The 20 km limit is applied to enhance a possible second peak between 150 and 750 ms as evidenced in the analysis of the TGF sample. The four panels have different thresholds on peak currents for the first stroke. The same analysis was also performed, with similar results as GLD360, for WWLLN data without any selection on polarity and peak current, because these variables are not available for WWLLN data. If the second peak is a general characteristic of +IC flashes, selection based on polarity and peak current of the flash as reported by GLD360 are not adequate enough to identify the second peak univocally in this sample.

As we could not identify a general second peak in the lightning data it seems that the second peak is not evident for flashes in general, thus suggesting that the second peak is a characteristic feature of a significant fraction of flashes that start with a TGF. Contrary to the blind search lightning flash sample (Figure 6), the TGF flashes (Figure 1) show a sharp decay after the first stroke which is not evident in the blind search sample. This suggests that those strokes with a TGF represent a large discharge and that it takes more than 150 ms before the electric activity is reactivated.
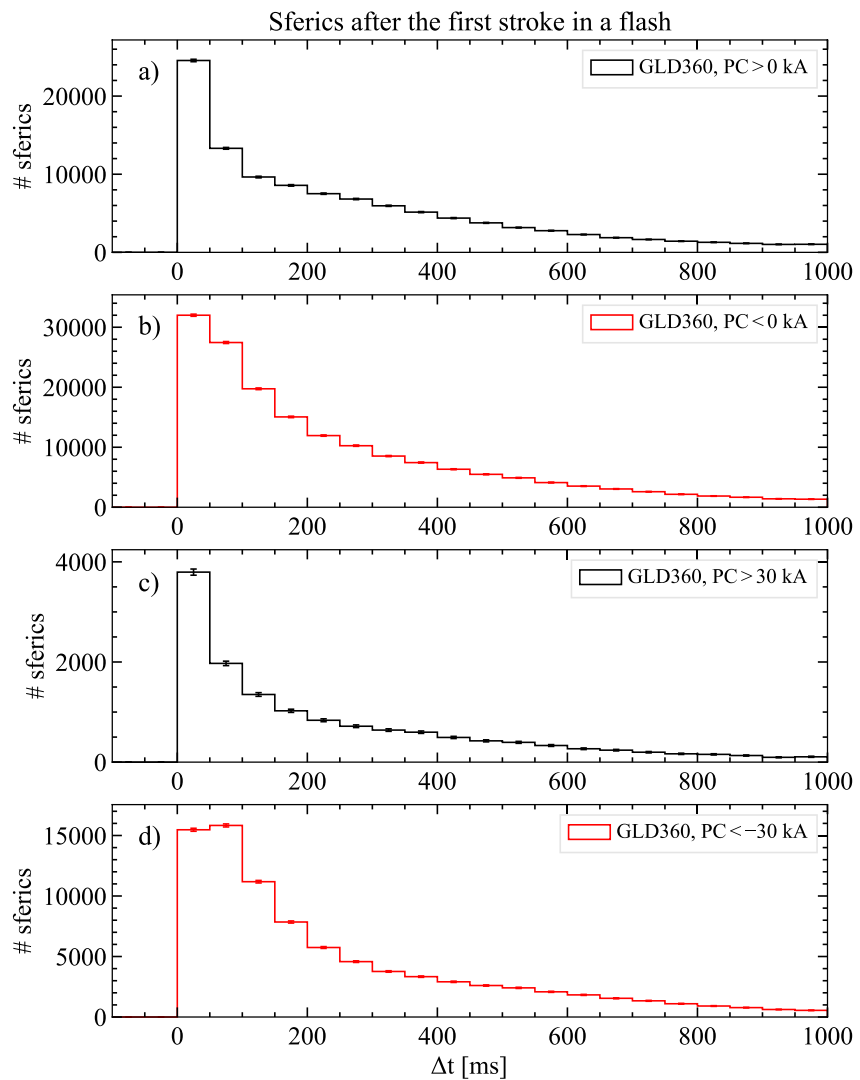
Figure 6. Histograms showing sferics within 20 km of the first stroke in a lightning flash. The first stroke is defined as the first sferic within a radius of 800 km with no detected sferics up to 2 s before. The first stroke itself is not included in the plot. The bin size is 50 ms. Each panel has a criterion, shown in the legend, on the peak current of the first stroke in the flash. The uncertainty of the data points is ±1 standard deviation assuming Poisson statistics.

5. Summary

The TGF catalogs of RHESSI, Fermi, AGILE, and ASIM, a total of over 5,000 TGFs with sferic data ±4 s within 500 km from the subsatellite point, are used to investigate the correlation between TGFs and sferics. The temporally closest sferic to the TGF has been studied in detail before (Albrechtsen et al., 2019; Connaughton et al., 2010, 2013; Lindanger et al., 2020; Marisaldi et al., 2015; Mezentsev et al., 2016; Østgaard et al., 2015), but the focus in these previous works was to find the *temporally closest* sferic associated to the TGF. In this study we have taken into account *all* sferics temporally close to the TGF. The study supports the idea that the TGFs are produced in the beginning of the lightning flash.

The conclusion is also supported by data from the ASIM instrumental suite, that provide a detailed high resolution data set combining TGF gamma-ray detection and optical lightning measurements. 98% (57 events out of 58) of the TGFs, where we only have optical data from the TGF location, show no lightning activity before the TGF. In the 98% sample, 26% have only one measured optical pulse and 74% have several optical pulses following the TGF. For one event of the 58 TGF events there is flash activity prior to the TGF. However, we cannot rule out that this event is a time coincidence and that the TGF is not associated with the optical signal.

There is an excess of sferics detected 150–750 ms after the TGFs in agreement with Omar et al. (2014); Smith et al. (2016). We term this excess of sferics the second peak. This study shows that in general the second peak is co-located with the first peak within <20 km, meaning that the discharges producing the second peak are co-located with the production location of the TGFs within the spatial uncertainties of the lightning detection networks. For TGFs associated with WWLLN, on average 13% of the TGFs with a WWLLN-sferic match have sferics in the second peak. For GLD360 and ASIM TGFs this fraction grows to 51%, showing that the presence or not of sferics in the second peak is strongly dependent on the sensitivity of the lightning network. A blind search in the lightning data, investigating if the second peak is a general property of lightning flashes, shows no evidence of a second peak for various selections on peak current. This suggests that the second peak is a characteristic feature for some lightning flashes that start with a TGF.

Data Availability Statement

WWLLN and VAISALA data are available upon subscription. ASIM is a mission of the European Space Agency (ESA) and is funded by ESA and by national grants of Denmark, Norway and Spain. ASIM data used for this study are available from the authors upon reasonable request or can be downloaded from the ASIM Science Data Center (https://asdc.space.dtu.dk). The RHESSI, Fermi, and AGILE TGF catalogs are available from the following links: https://scipp.pbsci.ucsc.edu/rhessi/, https://fermi.gsfc.nasa.gov/ssc/data/access/gbm/tgf/, and https://www.ssdc. asi.it/mcal3tgfcat/. Additional data for this paper are available at https://doi.org/10.5281/zenodo.5493848.

References

Abarca, S. F., Corbosiero, K. L., & Galarneau, Jr.,T. J. (2010). An evaluation of the Worldwide Lightning Location Network (WWLLN) using the National Lightning Detection Network (NLDN) as ground truth. *Journal of Geophysical Research*, *115*(D18). https://doi.org/10.1029/2009JD013411

Albrechtsen, K. H., Østgaard, N., Berge, N., & Gjesteland, T. (2019). Observationally weak TGFs in the RHESSI data. *Journal of Geophysical Research: Atmospheres*, *124*(1), 287–298. https://doi.org/10.1029/2018JD029272

Bogomolov, V. V., Panasyuk, M. I., Svertilov, S. I., Bogomolov, A. V., Garipov, G. K., Iyudin, A. F., et al. (2017). Observation of terrestrial gamma-ray flashes in the RELEC space experiment on the Vernov satellite. *Cosmic Research*, *55*(3), 159–168. https://doi.org/10.1134/S0010952517030017

Briggs, M. S., Xiong, S., Connaughton, V., Tierney, D., Fitzpatrick, G., Foley, S., et al. (2013). Terrestrial gamma-ray flashes in the Fermi era: Improved observations and analysis methods. *Journal of Geophysical Research: Space Physics*, *118*(6), 3805–3830. https://doi.org/10.1002/jgra.50205

Bürgesser, R. E. (2017). Assessment of the world wide lightning location network (WWLLN) detection efficiency by comparison to the Lightning Imaging Sensor (LIS). *Quarterly Journal of the Royal Meteorological Society*, *143*(708), 2809–2817. https://doi.org/10.1002/qj.3129

Chanrion, O., Neubert, T., Lundgaard Rasmussen, I., Stoltze, C., Tcherniak, D., Jessen, N. C., et al. (2019). The Modular Multispectral Imaging Array (MMIA) of the ASIM payload on the International Space Station. *Space Science Reviews*, *215*(4), 28. https://doi.org/10.1007/s11214-019-0593-y

Collier, A. B., Gjesteland, T., & Østgaard, N. (2011). Assessing the power law distribution of TGFs. *Journal of Geophysical Research*, *116*(A10). https://doi.org/10.1029/2011JA016612

Connaughton, V., Briggs, M. S., Holzworth, R. H., Hutchins, M. L., Fishman, G. J., Wilson-Hodge, C. A., et al. (2010). Associations between Fermi gamma-ray burst Monitor terrestrial gamma ray flashes and sferics from the world wide lightning location network. *Journal of Geophysical Research*, *115*(A12). https://doi.org/10.1029/2010JA015681

Connaughton, V., Briggs, M. S., Xiong, S., Dwyer, J. R., Hutchins, M. L., Grove, J. E., et al. (2013). Radio signals from electron beams in terrestrial gamma ray flashes. *Journal of Geophysical Research: Space Physics*, *118*(5), 2313–2320. https://doi.org/10.1029/2012JA018288

Cummer, S. A., Lu, G., Briggs, M. S., Connaughton, V., Xiong, S., Fishman, G. J., & Dwyer, J. R. (2011). The lightning-TGF relationship on microsecond timescales. *Geophysical Research Letters*, *38*(14). https://doi.org/10.1029/2011GL048099

Cummer, S. A., Lyu, F., Briggs, M. S., Fitzpatrick, G., Roberts, O. J., & Dwyer, J. R. (2015). Lightning leader altitude progression in terrestrial gamma-ray flashes. *Geophysical Research Letters*, *42*(18), 7792–7798. https://doi.org/10.1002/2015GL065228

Cummer, S. A., Zhai, Y., Hu, W., Smith, D. M., Lopez, L. I., & Stanley, M. A. (2005). Measurements and implications of the relationship between lightning and terrestrial gamma ray flashes. *Geophysical Research Letters*, *32*(8). https://doi.org/10.1029/2005GL022778

Dwyer, J. R. (2003). A fundamental limit on electric fields in air. *Geophysical Research Letters*, *30*(20). https://doi.org/10.1029/2003gl017781

Dwyer, J. R., & Cummer, S. A. (2013). Radio emissions from terrestrial gamma-ray flashes. *Journal of Geophysical Research: Space Physics*, *118*(6), 3769–3790. https://doi.org/10.1002/jgra.50188

Dwyer, J. R., & Smith, D. M. (2005). A comparison between Monte Carlo simulations of runaway breakdown and terrestrial gamma-ray flash observations. *Geophysical Research Letters*, *32*(22). https://doi.org/10.1029/2005GL023848

Fishman, G. J., Bhat, P. N., Mallozzi, R., Horack, J. M., Koshut, T., Kouveliotou, C., et al. (1994). Discovery of Intense gamma-ray flashes of atmospheric Origin. *Science*, *264*(5163), 1313–1316. https://doi.org/10.1126/science.264.5163.1313

Gurevich, A., Milikh, G., & Roussel-Dupre, R. (1992). Runaway electron mechanism of air breakdown and preconditioning during a thunderstorm. *Physics Letters A*, *165*(5), 463–468. https://doi.org/10.1016/0375-9601(92)90348-p

Heumesser, M., Chanrion, O., Neubert, T., Christian, H. J., Dimitriadou, K., Gordillo-Vazquez, F. J., et al. (2021). Spectral observations of optical emissions associated with terrestrial gamma-ray flashes. *Geophysical Research Letters*, *48*(4), 2020GL090700. https://doi.org/10.1029/2020GL090700

Hutchins, M. L., Holzworth, R. H., Brundell, J. B., & Rodger, C. J. (2012). Relative detection efficiency of the world wide lightning location network. *Radio Science*, *47*(6), RS6005. https://doi.org/10.1029/2012rs005049

Lindanger, A., Marisaldi, M., Maiorana, C., Sarria, D., Albrechtsen, K., Østgaard, N., et al. (2020). The 3rd AGILE terrestrial gamma ray flash catalog. Part I: Association to lightning sferics. *Journal of Geophysical Research: Atmospheres*, *125*(11). https://doi.org/10.1029/2019JD031985

Lindanger, A., Marisaldi, M., Sarria, D., Østgaard, N., Lehtinen, N., Skeie, C. A., et al. (2021). Spectral analysis of individual terrestrial gamma-ray flashes detected by ASIM. *Journal of Geophysical Research: Atmospheres*, *126*(23), e2021JD035347. https://doi.org/10.1029/2021JD035347

Lu, G., Blakeslee, R. J., Li, J., Smith, D. M., Shao, X.-M., McCaul, E. W., et al. (2010). Lightning mapping observation of a terrestrial gamma-ray flash. *Geophysical Research Letters*, *37*(11). https://doi.org/10.1029/2010GL043494

Mailyan, B. G., Briggs, M. S., Cramer, E. S., Fitzpatrick, G., Roberts, O. J., Stanbro, M., & Dwyer, J. R. (2016). The spectroscopy of individual terrestrial gamma-ray flashes: Constraining the source properties. *Journal of Geophysical Research: Space Physics*, *121*, 11–346. https://doi.org/10.1002/2016ja022702

Mailyan, B. G., Nag, A., Dwyer, J. R., Said, R. K., Briggs, M. S., Roberts, O. J., et al. (2020). Gamma-ray and radio-frequency Radiation from thunderstorms observed from space and ground. *Scientific Reports*, *10*(1), 7286. https://doi.org/10.1038/s41598-020-63437-2

Maiorana, C., Marisaldi, M., Füllekrug, M., Soula, S., Lapierre, J., Mezentsev, A., et al. (2021). Observation of terrestrial gamma-ray flashes at mid latitude. *Journal of Geophysical Research: Atmospheres*, *126*(18). https://doi.org/10.1029/2020JD034432

Maiorana, C., Marisaldi, M., Lindanger, A., Østgaard, N., Ursi, A., Sarria, D., et al. (2020). The 3rd AGILE terrestrial gamma-ray flashes catalog. Part II: Optimized selection criteria and characteristics of the new sample. *Journal of Geophysical Research: Atmospheres*, *125*(11). https://doi.org/10.1029/2019JD031986

Marisaldi, M., Argan, A., Ursi, A., Gjesteland, T., Fuschino, F., Labanti, C., et al. (2015). Enhanced detection of terrestrial gamma-ray flashes by AGILE. *Geophysical Research Letters*, *42*(21), 9481–9487. https://doi.org/10.1002/2015GL066100

Marisaldi, M., Fuschino, F., Labanti, C., Galli, M., Longo, F., Del Monte, E., et al. (2010). Detection of terrestrial gamma ray flashes up to 40 MeV by the AGILE satellite. *Journal of Geophysical Research*, *115*(A3). https://doi.org/10.1029/2009JA014502

Marisaldi, M., Galli, M., Labanti, C., Østgaard, N., Sarria, D., Cummer, S. A., et al. (2019). On the high-energy spectral Component and fine time Structure of terrestrial gamma ray flashes. *Journal of Geophysical Research: Atmospheres*, *124*(14), 7484–7497. https://doi.org/10.1029/2019JD030554

Mezentsev, A., Østgaard, N., Gjesteland, T., Albrechtsen, K., Lehtinen, N., Marisaldi, M., et al. (2016). Radio emissions from double RHESSI TGFs. *Journal of Geophysical Research: Atmospheres*, *121*(13), 8006–8022. https://doi.org/10.1002/2016JD025111

Neubert, T., Østgaard, N., Reglero, V., Blanc, E., Chanrion, O., Oxborrow, C. A., et al. (2019). The ASIM mission on the International space station. *Space Science Reviews*, *215*(2), 26. https://doi.org/10.1007/s11214-019-0592-z

Neubert, T., Østgaard, N., Reglero, V., Chanrion, O., Heumesser, M., Dimitriadou, K., et al. (2020). A terrestrial gamma-ray flash and ionospheric ultraviolet emissions powered by lightning. *Science*, *367*(6474), 183–186. https://doi.org/10.1126/science.aax3872

Omar, K. S., Briggs, M. S., & Heckman, S. (2014). *Characterizing the TGF-lightning relationship using ENTLN*. AGU Fall Meeting.

Østgaard, N., Albrechtsen, K. H., Gjesteland, T., & Collier, A. (2015). A new population of terrestrial gamma-ray flashes in the RHESSI data. *Geophysical Research Letters*, *42*(24), 10–937. https://doi.org/10.1002/2015GL067064

Østgaard, N., Balling, J. E., Bjørnsen, T., Brauer, P., Budtz-Jørgensen, C., Bujwan, W., et al. (2019). The Modular X- and Gamma-Ray Sensor (MXGS) of the ASIM Payload on the International Space Station. *Space Science Reviews*, *215*, 23. https://doi.org/10.1007/s11214-018-0573-7

Østgaard, N., Cummer, S. A., Mezentsev, A., Luque, A., Dwyer, J., Neubert, T., et al. (2021). Simultaneous observations of EIP, TGF, Elve, and optical lightning. *Journal of Geophysical Research: Atmospheres*, *126*(11), e2020JD033921. https://doi.org/10.1029/2020JD033921

Østgaard, N., Gjesteland, T., Carlson, B. E., Collier, A. B., Cummer, S. A., Lu, G., & Christian, H. J. (2013). Simultaneous observations of optical lightning and terrestrial gamma ray flash from space. *Geophysical Research Letters*, *40*(10), 2423–2426. https://doi.org/10.1002/grl.50466

Østgaard, N., Neubert, T., Reglero, V., Ullaland, K., Yang, S., Genov, G., et al. (2019). First 10 Months of TGF observations by ASIM. *Journal of Geophysical Research: Atmospheres*, *124*(24), 14024–14036. https://doi.org/10.1029/2019JD031214

Roberts, O. J., Fitzpatrick, G., Stanbro, M., McBreen, S., Briggs, M. S., Holzworth, R. H., et al. (2018). The first Fermi-GBM terrestrial gamma ray flash catalog. *Journal of Geophysical Research: Space Physics*, *123*(5), 4381–4401. https://doi.org/10.1029/2017JA024837

Rodger, C. J., Brundell, J. B., Holzworth, R. H., Lay, E. H., Crosby, N. B., Huang, T.-Y., & Rycroft, M. J. (2009). Growing detection efficiency of the world wide lightning location network. *AIP Conference Proceedings*, *1118*(1), 15–20. https://doi.org/10.1063/1.3137706

Said, R. K., & Murphy, M. J. (2016). GLD360 Upgrade: Performance analysis and applications. In *24th International Lightning Detection Conference(IC)*.

Shao, X.-M., Hamlin, T., & Smith, D. M. (2010). A closer examination of terrestrial gamma-ray flash-related lightning processes. *Journal of Geophysical Research*, *115*(A6). https://doi.org/10.1029/2009JA014835

Smith, D. M., Buzbee, P., Kelley, N. A., Infanger, A., Holzworth, R. H., & Dwyer, J. R. (2016). The rarity of terrestrial gamma-ray flashes: 2. RHESSI stacking analysis. *Journal of Geophysical Research: Atmospheres*, *121*(19), 11–382. https://doi.org/10.1002/2016JD025395

Smith, D. M., Kelley, N. A., Buzbee, P., Infanger, A., Splitt, M., Holzworth, R. H., & Dwyer, J. R. (2020). Special Classes of terrestrial gamma ray flashes from RHESSI. *Journal of Geophysical Research: Atmospheres*, *125*(20), e2020JD033043. https://doi.org/10.1029/2020JD033043

Smith, D. M., Lopez, L. I., Lin, R. P., & Barrington-Leigh, C. (2005). Terrestrial gamma-ray flashes observed up to 20 MeV. *Science (New York, N.Y.)*, *307*, 1085–1088. https://doi.org/10.1126/science.1107466

Stanley, M. A., Shao, X. M., Smith, D. M., Lopez, L. I., Pongratz, M. B., Harlin, J. D., et al. (2006). A link between terrestrial gamma-ray flashes and intracloud lightning discharges. *Geophysical Research Letters*, *33*(6). https://doi.org/10.1029/2005GL025537

Ursi, A., Guidorzi, C., Marisaldi, M., Sarria, D., & Frontera, F. (2017). Terrestrial gamma-ray flashes in the BeppoSAX data archive. *Journal of Atmospheric and Solar-Terrestrial Physics*, *156*, 50–56. https://doi.org/10.1016/j.jastp.2017.02.014

Erratum

In the originally published version of this article, an interchange of two numbers in Section 3.2 was discovered. The following have since been corrected and this version may be considered the authoritative version of record.

In paragraph two (15 events) and (42 events) have been switched to reflect the correct number and what is clear from the rest of the discussion and summary.

In paragraph three the event number has been changed to (out of 42) to reflect the correct number and what is clear from the rest of the discussion and summary.